Phase separation in Fe-Si and Co-Si sputtered ferromagnetic alloys and the origin of their magnetic anisotropy

J. Díaz,* R. Morales, S. M. Valvidares, and J. M. Alameda
Departamento de Física, Universidad de Oviedo, Avenida de Calvo Sotelo s/n, Oviedo-33007, Spain
(Received 23 December 2004; revised manuscript received 28 July 2005; published 12 October 2005)

Fe-Si and Co-Si thin films were studied with different Si concentrations by x-ray absorption spectroscopy (XAFS), and the analysis was confronted to their magnetic properties of coercivity and anisotropy. The analysis of the XAFS spectra showed a higher disorder in the amorphous Fe-Si films than in the Co-Si films and a larger degree of clustering of Co atoms, consistent with the higher heat of alloying of Fe-Si with respect to Co-Si alloys. Both kinds of amorphous films contained a strongly disordered silicide phase that was hardly detected by extended XAFS spectroscopy (EXAFS). EXAFS spectra were dominated by the nonmagnetic $(Fe,Co)Si_2$ environments. The orientation of the magnetic easy axis of the films was correlated with the expected anisotropic spatial distribution of Si concentration, which was defined by the oblique angle of incidence of Si atoms during film deposition. This indicates that such a detected nonmagnetic Si rich environments were anisotropically distributed and possibly segregated, influencing in a significant way the magnetic anisotropy of these films.

DOI: 10.1103/PhysRevB.72.144413 PACS number(s): 75.30.Gw, 75.50.Kj, 75.50.Bb, 61.10.Ht

I. INTRODUCTION

The starting model to explain the magnetic anisotropy and coercivity in amorphous alloys is to consider the competition between the ferromagnetic exchange interaction and the uniaxial magneto-crystalline anisotropy of each atomic site.[1,2] In the case of Transition Metals-Metalloid (TM-M) alloys, the magneto-crystalline anisotropy is notably reduced because the 3*d* electrons interact strongly with the crystal field and their spin-orbit interaction is relatively weak. Their magnetic properties should be largely determined by the exchange interaction. Ideally, a total random arrangement of atoms in these alloys should reduce their coercive field and anisotropy energy to negligible values.[2] Therefore, the control of the magnitude of these magnetic properties needs to know how much they can be affected when the atomic arrangement in this kind of alloy deviates from the ideal homogeneous atomic distribution.

TM-M alloys are prepared by different methods, either by thin film growth on a substrate, or by rapid quenching from a melt to prevent crystallization, usually taking the form of ribbons. Thin film deposition allows us to extend the concentrations in which amorphous alloys can be produced compared to the rapid quenching procedure. Also, this method permits us to introduce anisotropies in a rather controlled way. For instance, by externally applying magnetic fields during deposition[3] or evaporating at oblique angles.[4] The highest disorder is usually obtained when the relative concentration is near the deepest eutectic point of the mixture.[5,6] Phase separation is expected for concentrations above and below such a point.[7]

Buschow *et al.*[8–10] showed experimental indications two decades ago that the presence of a some amount of compositional short range order in these alloys would have a relatively large weight in the determination of their magnetic properties, namely the magnitude of the magnetic moment of the TM atom. He proposed that positive values of heat in mixing will lead to some clustering between like atoms, and negative values to clustering between unlike atoms. Co-Si and Fe-Si alloys are, in this sense, interesting to compare. They have a similar deep-eutectic in their phase diagram, but they differ in their formation enthalpy.[11] Co-Co bonds have an enthalpy larger than Fe-Fe. And Co-Si bonds have a lower formation enthalpy than Fe-Si bonds. Therefore, it is expected for a larger segregation of Co-Co bonds compared to Fe-Fe in these kind of alloys.[8,10] Actually, the different behavior of Fe and Co in the presence of Si has been already observed by XAFS spectroscopy in other systems.[12,13]

Another important difference between both alloys noticed in our laboratory is their magnetic anisotropy, especially its direction, when they are deposited on a substrate by evaporation. Both kinds of amorphous alloys are magnetically uniaxial, with their anisotropy axis always laying in the plane. In the case of the Co-Si alloys, the easy axis is defined by the plane of incidence of the evaporated species for any Si concentration.[4,14] However, the Fe-Si amorphous alloys have a range of low Si concentrations where their easy axes does not point in such a direction,[15] and it can be oriented by externally applied magnetic fields of weak intensity (lower than 30 Oe) during film deposition. Since the anisotropy of Co-Si films, and Fe-Si with high enough Si concentrations, is unchanged by externally applied magnetic fields, it is proposed that its origin should be associated to the internal structure of the film. Such a structure would probably be derived from fluctuations in the Si concentration, possibly at the nanometer scale,[16] where segregated nonmagnetic or poorly magnetic regions rich in Si would surround magnetic regions rich in Fe.[15,17] To determine the presence of such a possible segregation and its influence in the coercivity and anisotropy properties of these alloys, several films were deposited with Si concentrations above and below the amorphous concentration. The levels of such a segregation were measured by EXAFS spectroscopy, which is very sensitive to ordered atomic environments and much less sensitive to disordered or liquid-like environments.[18–23]

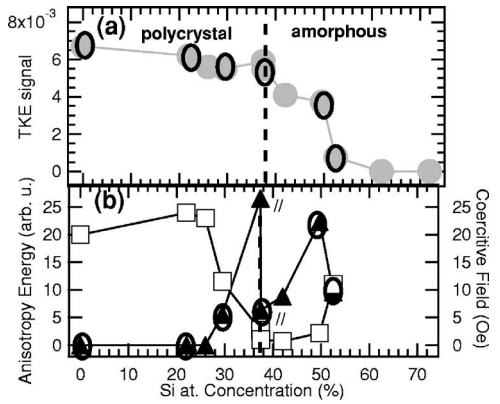

FIG. 1. (a) Transversal Kerr Effect(TKE) signal vs the atomic concentration of Si in the Fe-Si films; (b) coercitive field (empty squares) and anisotropy energy factor (solid triangles) vs the atomic concentration of Si in the Fe-Si films. The samples analyzed by XAFS spectroscopy were signaled with an ellipsoid in both figures. The symbol ‖ in (b) indicates the sample with magnetic anisotropy parallel to evaporation plane (see text).

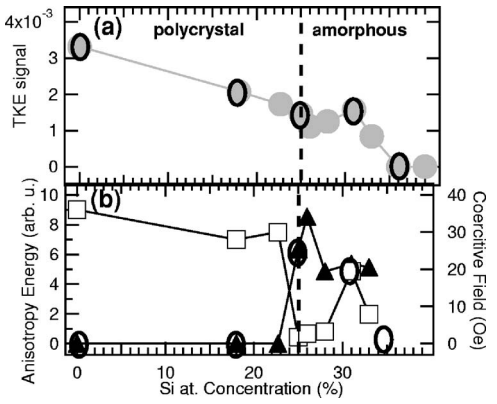

FIG. 2. (a) Transversal Kerr Effect(TKE) signal versus the atomic concentration of Si in the Co-Si films; (b) coercitive field (empty squares) and anisotropy energy factor (solid triangles) versus the atomic concentration of Si in the Co-Si films. The samples analyzed by XAFS spectroscopy were signaled with an ellipsoid in both figures.

II. EXPERIMENTAL DETAILS

The thin films were obtained by co-deposition of Co, Fe, and Si by DC magnetron sputtering on polished fused quartz substrates, cut from the same piece, to minimize substrate contributions to the XAFS spectra. They were grown at room temperature with a sputtering Ar pressure of 1×10^{-3} mbar, with a system base pressure of 1×10^{-8} mbar. Thickness of films were 200 nm. The composition was varied controlling the relative power of the magnetrons. The angle of incidence of sputtered atoms with respect to the normal substrate was 0° for Fe and Co atoms and 36° for Si atoms. The distance from sample to target was 20 cm and the deposition rate was 0.1 nm/s, measured with a quartz balance.

Hysteresis loops of the samples were measured at RT by the Magneto-Optical Transversal Kerr effect (TKE) using white light from an halogen lamp. Magnetic fields applied during TKE measurements were always in the plane of the sample, and either parallel or perpendicular to the plane of incidence of the light. This allowed us to measure the components of the magnetization of the sample parallel ($M\|$) and perpendicular ($M\perp$) to the applied field for a certain orientation of the easy axis with respect to the magnetic field. For a given easy axis orientation, the ($M\|$) component was obtained applying the magnetic field perpendicularly to the plane of incidence of the light. The ($M\perp$) component was recorded rotating the sample 90° and applying the magnetic field parallel to the plane of incidence of the light. The relative magnetization of the samples were obtained from the saturation of their hysteresis loops. Their coercitive and anisotropy fields, H_c and H_k, displayed in Figs. 1 and 2, were obtained from the hysteresis loops of the component of the magnetization parallel to the applied magnetic field ($M\|$). H_c was extracted from the hysteresis loop recorded with the magnetic field parallel to the easy axis, and H_k from the hysteresis loop measured parallel to the hard axis.

Fe and Si concentration in the samples were determined by x-ray photoemission spectroscopy (XPS). The atomic structure of the films was studied by x-ray diffraction, and XAFS spectroscopy. XAFS experiments were performed at the ESRF synchrotron, at GILDA beam line. X-ray absorption detection was done at liquid nitrogen temperature measuring the total fluorescence yield using a Ge detector. The EXAFS spectra were acquired up to 800 eV above the Fe edge (7100 eV) and the Co edge (7700 eV). Therefore, the range of *k-space* covered extended up to 14 $Å^{-1}$.

III. RESULTS AND DISCUSSION

A. Magnetic properties: Hysteresis loops

Figure 1 shows the coercitive and anisotropy fields, and the TKE signal vs Si concentration for the measured Iron films and Fig. 2 for the Cobalt Silicide thin films. The transition from polycristalline to the amorphous region, determined by XRD and XAFS, occurred at lower Si concentrations for the Co-Si films, about 25% at. Si, than for Fe-Si films, 35% at. Si, in coincidence with the concentrations where their corresponding deep eutectic point are found in their phase transition diagrams. Above such concentrations, the coercitive field dropped to the lowest values, and the films became magnetically uniaxial, increasing their anisotropy energy. The anisotropy factor A_u represented in Figs. 1 and 2 was the anisotropy field H_k multiplied by the TKE signal. Therefore, A_u was proportional to the anisotropy energy K_u, assuming that the TKE signal was proportional to the magnetization of the sample.[24] The anisotropy energy of the most anisotropic amorphous Fe-Si film was[15] 2×10^4 erg/cm^3 and in the amorphous Co-Si film was[14] 6×10^3 erg/cm^3.

The magnetic anisotropy of the easy axis of the amorphous films was always in the plane of the sample and, for most of the films, it pointed perpendicular to the plane of incidence of the evaporated atoms. There was an important exception that occurred only in the Fe silicide films. Their easy axis was perpendicular to the evaporation plane only when the Si concentration was higher than about 40%. For Si

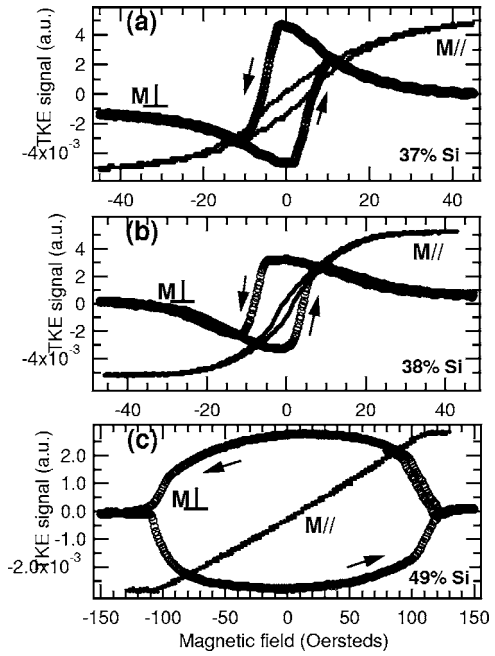

FIG. 3. Hysteresis loops of the $M\|$ and $M\perp$ components of Fe-Si amorphous thin films measured by TKE with the magnetic field applied along the hard axis. (a) Sample with easy axis nearly parallel to the incidence plane of evaporation; (b) Sample with easy axis in the same direction as the previous one but with lower magnetic anisotropy; and (c) Sample with higher Si at. concentration. Its easy axis was perpendicular to the incidence plane of evaporation. The Si concentrations of each sample was indicated in the right corner of the corresponding figure.

concentrations near the polycrystalline to amorphous transition, their easy axis pointed rather parallel to the plane of evaporation. Since comparisons between both kind of samples will be done along this paper, the magnetic samples with the magnetic anisotropy parallel to the evaporation plane will be abbreviated with the acronym PEP, and those with the anisotropy perpendicular (or anti-parallel) to the evaporation plane, AEP. Both kinds of samples have a different behavior under externally applied magnetic fields during film deposition. PEP samples aligned their magnetic easy axis with the direction of the applied magnetic field, even if its intensity was lower than their anisotropy fields H_k. Such an effect was not produced in the AEP samples, even if the intensity of the applied fields was higher than their anisotropy field H_k.

The hysteresis loops of the easy axis along the $M\|$ component of the magnetization were squared in the PEP and AEP samples, with $M\|_r/M\|_s$ close to 1, showing a marked uniaxial behavior. Differences were more visible in the hysteresis loops of the hard axis. Figure 3 shows the hysteresis loops for the components of the magnetization parallel ($M\|$) and perpendicular ($M\perp$) to the applied field and the hard axis of two PEP samples [Figs. 3(a) and 3(b)] and one AEP sample [Fig. 3(c)]. The hysteresis loop of the $M\|$ component in the PEP samples had some magnetic remanence and the approach of the magnetization to saturation had a significant curvature, possibly caused by a larger dispersion in the magnitude and the orientation of the magnetic anisotropy over the film. The same kind of hysteresis loop of the AEP sample had negligible remanence, and the magnetization varied almost linearly, indicating little dispersion in the anisotropy orientation. The strong change in the anisotropy energy of the Fe-Si films with PEP anisotropy observed in Fig. 1 (37% and 38% Si at.) was probably due to the presence of the two kind of anisotropies PEP and AEP in the films. Since they are perpendicular, both compete in the definition of the easy axis direction of the film. Therefore, the film with PEP anisotropy with the lowest anisotropy energy (38% at.) should be the one with the highest AEP component.

The hysteresis loops of the hard axis in the $M\perp$ component evidenced differences in the magnetization process between both kind of samples as well. These hysteresis loops were measured with the hard axis less than 5° misaligned to the applied magnetic field, since $M\perp$ is close to zero when the field is perfectly aligned to the hard axis. The $M\perp$ of the PEP samples [Figs. 3(a) and 3(b)] switched their orientation at magnetic fields much lower than the anisotropy fields. Also, the PEP sample with the lowest anisotropy [Fig. 3(b)] never reached the saturation magnetization at zero field in these loops, meaning that a part of the sample broke in antiparallel domains. Both facts are an indication that the samples had a certain dispersion in the orientation of their anisotropy axes. On the other hand, the magnetization process of the AEP samples was of films with a very well defined magnetic anisotropy axis. Their $M\perp$ component reached saturation at zero field, and the field that switched their $M\perp$ component was closed to the anisotropy field. In some of the samples, as the one in Fig. 3(c), never switched their $M\perp$, i.e., their magnetization simply rotated 180°, as a monodomain. Samples approached such a behavior with increasing Si concentration.

The amorphous Co-Si films had similar hysteresis loops than the AEP Fe-Si films. Figures 4(b) and 4(c) are the hard axis hysteresis loops ($M\perp$ and $M\|$ components) of two amorphous Co-Si films. Sample in Fig. 4(b) had a Si concentration of 25% at. Si and sample in Fig. 4(c) had 33% at. Si. The comparison between both figures shows that the 180° rotation of the magnetization occurs in the more silicided film. Note from Fig. 2 that the coercitivity field H_c increases with increasing Si concentration as well, with one exception. The increase in H_c does not come from an increase in the anisotropy energy (see Fig. 1), suggesting that increasing the Si concentration in the films increases the density of defects that causes pinning of the domain walls.

By contrast, similar hysteresis loops of the $M\perp$ component measured in the polycrystalline samples had a much lower intensity at zero field compared to the amorphous films. This can be seen in Fig. 4(a), which shows the hysteresis loops of the $M\perp$ and $M\|$ components of a polycrystalline Co-Si film. This is mostly due to the higher dispersion in the local magnetic anisotropy of the polycrystalline samples,[14,25] as it has been evidenced by transversal susceptibility measurements,[26] which showed a significant magnetic ripple[26–28] for the polycrystalline films[14] and almost negligible for the amorphous films.[15] The local anisotropy in polycrystals is determined by the orientation of each of the crystallites in the films, which, in the present case, were randomly oriented. In the amorphous films, the local anisotropy

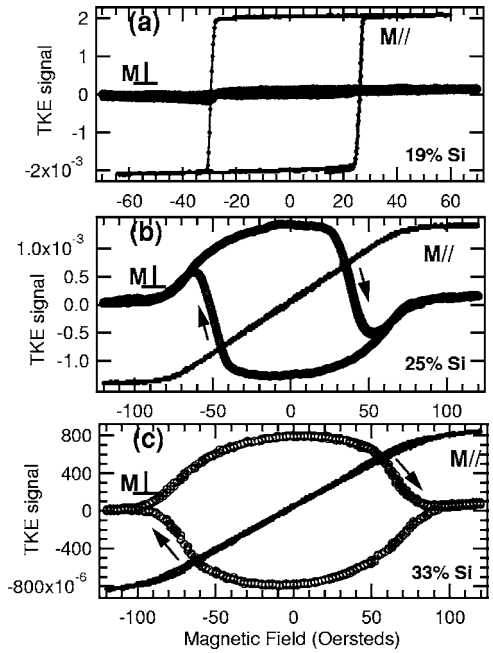

FIG. 4. Hysteresis loops of the $M\parallel$ and $M\perp$ components of Co-Si thin films measured by TKE with the magnetic field applied along the hard axis. (a) Polycrystalline sample; (b) Amorphous sample with easy axis in the direction perpendicular to the incidence plane of evaporation. (c) Sample with higher Si at. concentration. Its easy axis was also perpendicular to the incidence plane of evaporation. The Si concentrations of each sample was indicated in the right corner of the corresponding figure.

unit should be an atomic pair. The orbital momentum per magnetic atom, usually associated to the local magnetic anisotropy,[29] was quite high in the Fe-Si films when measured by X-ray Magnetic Dichroism.[15] But the relatively low magnetic anisotropy energy found in these films and the practical absence of magnetic ripple in them suggest that this apparent local atomic anisotropy has relatively little influence in the macroscopic anisotropy. Rather, it seems that it is the exchange coupling between atoms what dominates their magnetic anisotropy.

B. X-ray diffraction

The x-ray diffraction $\theta-2\theta$ scans of Co and Fe silicide polycrystalline films are plotted in Figs. 5 and 6. They were normalized to the intensity of the x-ray reflection from the substrate to be able to compare diffracted intensities between different samples.

Pure Iron films in the polycrystalline region had a single reflection at $2\theta=44.8°$ corresponding to a bcc structure with a $\langle 100\rangle$ texture. This peak upward shifted to $2\theta=45.2°$ with higher Si concentrations, corresponding to a reduction in the interatomic distances from 2.86 to 2.83 Å between second neighbors. Also, the intensity of this peak decreased significantly with increasing Si concentration, with little change in its width. Such a decrease in intensity cannot be attributed to changes in the texture of the film, as deduced from their rocking curves, plotted in Fig. 7, which did not show significant variations with Si content in the films.

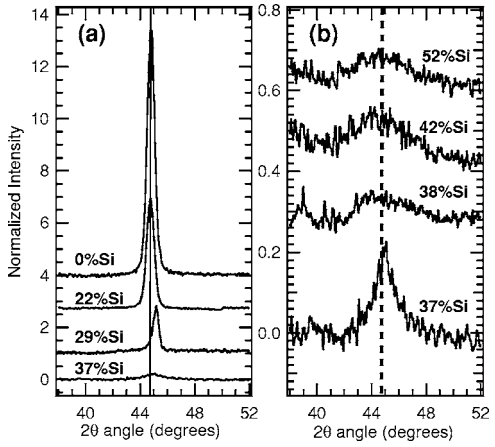

FIG. 5. $\theta-2\theta$ scans of the Fe-Si (a) polycystalline and (b) amorphous thin films. The diffracted intensity of the films was normalized to the diffracted intensity of the substrate. A constant was added to the scans for a better view. %Si are the atomic concentrations in the films.

There were more than one peak diffracted in the Co silicides films. The most intense of these peaks was centered at $2\theta=44.5°$. This peak is very close to the $\langle 111\rangle$ reflection in fcc-Co and the $\langle 002\rangle$ reflection in hcp-Co ($2\theta=44.36°$ and 44.8°, respectively). The peak corresponding to the $\langle 100\rangle$ reflection of hcp-Co, centered at $2\theta=41.8°$, was present at any Si concentration and it was unshifted. This suggests for the polycrystalline films a microstructure composed of a mixture of fcc and hcp phases, probably caused by a significant density of defects in the form of stacking faults.[14,30] The intensity of the x-ray diffracted peaks increased moderately with increasing Si concentration, following a behavior similar to the one observed by Fallon *et al.*[31] In that case, this increase in intensity was explained by an increase in the texture of the films with Si content. The present analyzed samples showed little changes in their rocking curves of the

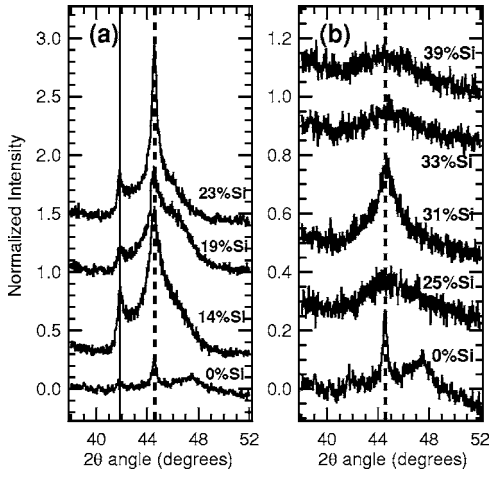

FIG. 6. $\theta-2\theta$ scans of the Co-Si (a) polycystalline and (b) amorphous thin films. The diffracted intensity of the films was normalized to the diffracted intensity of the substrate. A constant was added to the scans for a better view. %Si are the atomic concentrations in the films.

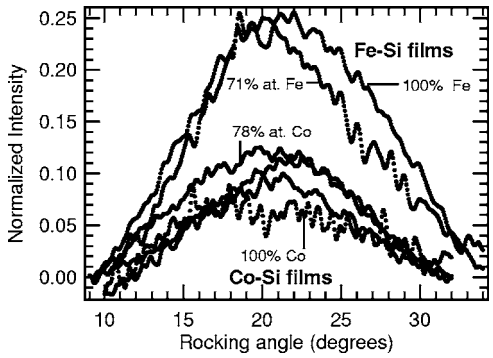

FIG. 7. Rocking curves of the Fe-Si and Co-Si polycrystalline thin films obtained at the ⟨110⟩ bcc-Fe reflection in the Fe-Si films and at the ⟨002⟩ hcp-Co reflection in the Co-Si films.

most intense peak at $2\theta=44.5°$, as it can be appreciated in Fig. 7. On the other hand, the change in shape of the spectra, especially the vanishing of the ⟨101⟩ peak and the increase of the ⟨100⟩ peak, both related to the hcp-Co structure, indicated a certain change in the crystalline texture of the films.

The intensity of the peaks in any of the Co silicide films are one order of magnitude smaller than the bcc reflection in the pure Fe film. Comparison of their respective rocking curves shown in Fig. 7 tells that this is because Fe-Si films were significantly more textured than Co-Si films. Experimental studies have related the crystalline texture of deposited metals with their reactivity with the substrate.[32,33] So the more exothermic is the reactivity between the components of the alloy and/or the substrate, the more textured is the film. Therefore, the difference between texture in Co-Si and Fe-Si is a consequence of the higher reactivity of Fe than Co with Si deduced from their estimated heats of alloying.[11]

X-ray diffracted intensity was almost vanished in both Iron and Cobalt amorphous silicides (see Figs. 5 and 6). Their diffracted halos were centered at $2\theta=45°$ in the Fe-Si film, and at $2\theta=44.7°$ in the Co-Si film, i.e., closer to the main reflections from their respective TM stable crystalline structures, bcc for Fe, hcp for Co.

C. XANES

Figures 8 and 9 compare the x-ray absorption spectra of several Fe-Si and Co-Si films with different Si content. The polycrystalline samples were perfectly distinguishable from the amorphous films because of their more structured EXAFS signal. The shape of the spectra of the polycrystalline alloys was very similar, especially the EXAFS region. It decreased in amplitude and smoothed its fine structure with increasing Si concentration. This qualitatively means that the structure of the polycrystalline silicide films was similar to that of the pure transition metal. The only important change caused by increasing the concentration of Si in the films appeared in their near edge region of the spectra (XANES). In the case of the Fe-Si films, the wide feature at about 40 eV from the edge, at 7160 eV, in the spectrum of the pure Fe film was split in two in the other two spectra corresponding to the polycrystalline silicide films. The valley between the two split peaks at 7160 eV coincides with the dip in

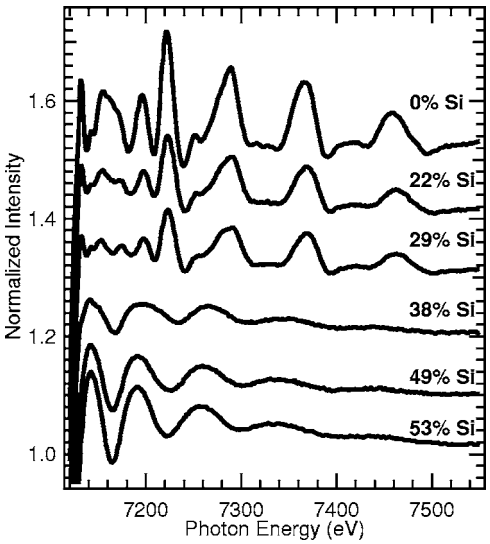

FIG. 8. XAFS spectra of the Fe-Si films. %Si are the atomic concentrations in the films.

intensity of the XANES spectrum of the Fe-Si amorphous alloys. Actually, the sum of the spectra of pure Fe with that of the amorphous alloy with the highest Si concentration, shown in Fig. 10(a), reproduce the split of the wide feature at 7160 eV. This suggests that, in the analyzed polycristalline silicides, two different Fe environments appeared: One equivalent to that of bcc Fe. The other disordered and rich in Si.

The XANES spectra of the Fe-Si amorphous alloys increase in amplitude with increasing Si concentration, inverse to the trend observed in the polycrystalline films. On the other hand, fine structure in the XANES spectra vanished with increasing Si content. This fine structure had its features at similar energies than in pure Fe only in the amorphous films with the lowest Si concentrations. Figure 10(b) compares the XANES spectrum of the amorphous alloy with the lowest Si concentration, with the sum of the pure Fe spec-

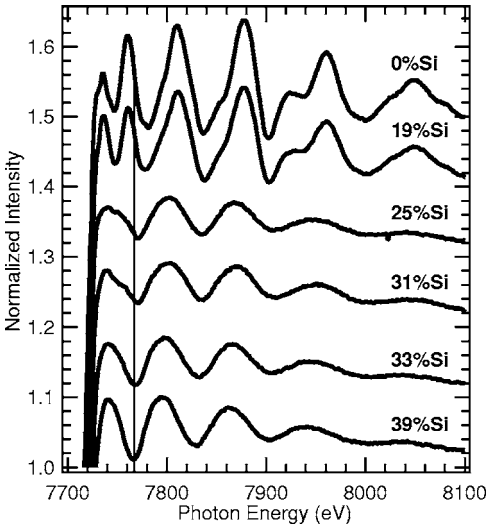

FIG. 9. XAFS spectra of the Co-Si films. %Si are the atomic concentrations in the films.

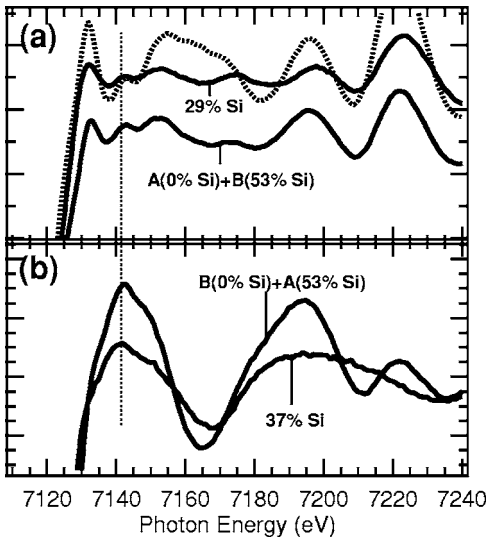

FIG. 10. (a) Comparison between the XANES spectra of the polycrystalline Fe-Si thin film with 29% at. Si concentration and the resulting from adding the spectrum of the pure Fe thin film (dashed line) and that of the most silicide Fe-Si amorphous film (53% at. Si), heavily weighting the former one. (b) Comparison between the XANES spectra of the amorphous Fe-Si thin film with 38% at. Si concentration and the resulting from adding the spectrum of the pure Fe thin film and that of the most silicide Fe-Si amorphous film (53% at. Si), heavily weighting the last one.

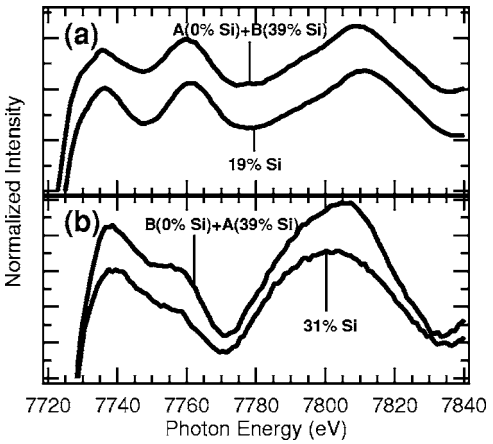

FIG. 11. (a) Comparison between the XANES spectra of the polycrystalline Co-Si thin film with 19% at. Si concentration and the resulting from adding the spectrum of the pure Co thin film and that of the most silicide Co-Si amorphous film (39% at. Si), heavily weighting the former one. (b) Comparison between the XANES spectra of the amorphous Co-Si thin film with 31% at. Si concentration and the resulting from adding the spectrum of the pure Co thin film (dashed line) and that of the most silicide Co-Si amorphous film (39% at. Si), heavily weighting the last one.

trum and that of the amorphous alloy with the highest Si concentration, which is featureless. The sum was done giving more weight to the spectra of the amorphous alloy. The fine structure in the XANES part of the spectrum is not so well reproduced as in the previous case, conveying that most of the pure Fe was mixed with Si at such a Si concentration. Still, it could be said that this spectrum retains some pure Fe features: It can be seen intuitively that the spectra would match if features of the pure Fe spectrum were conveniently broadened, especially if the two peaks at about 7190 and 7225 eV were broadened enough to become a single broad peak.

The XANES spectrum of the polycrystalline cobalt silicide resembled that of pure Co. The second broad peak, centered at 7761 eV, approximately at the same distance from the edge than in Fe, was not split, as observed in the Fe-Si films, but it had a lower intensity. However, note that the valleys of the EXAFS oscillations almost coincide in all the samples. Figure 11(a) show that the XANES spectrum of the polycrystalline silicide film can be obtained from the sum of the spectrum of the most silicide amorphous sample and that of the pure Co film.

The XANES spectra of the amorphous cobalt alloys showed a similar behavior than that observed in the amorphous Fe-Si films. They smoothed with increasing Si content until they became featureless at the highest Si concentration. Also, the features observed in them could be associated to hcp-Co. This can be seen in Fig. 11(b), where the XANES spectrum with low Si content is compared with the result from the sum of the spectrum of the most siliced alloy and the spectrum of pure Co, heavily weighting the former in the sum. Note that the match is remarkably better in this case than in the Fe-Si films. Actually, the analysis of the EXAFS part of the spectra showed that the mixing of Fe with Si was stronger than in the Cobalt silicide films.

D. EXAFS

1. Polycystalline films

Figures 8 and 9 show that the EXAFS spectra of the polycristalline samples evolved in a similar way with increasing Si content in both kind of alloys: The shape of the spectra remained almost invariable but the amplitude decreased. This can be seen better in Figs. 12 and 13. The spectra $\Phi(R)$ of the samples with different Si concentrations plotted in these figures is the Fourier transform of their respective EXAFS signal, $\chi(k)$, where k is the momentum of the scattered electron, i.e., $k=\sqrt{(E_0-E)/\hbar}$. E_0 is the photon energy at the absorption edge. In this case, $\chi(k)$ was multiplied by k^2 to enhance the part of the spectra with higher k values, i.e., $\Phi(R)=F[k^2\chi(k)]$. $\Phi(R)$ is closely related to the radial distribution of atoms around the excited atom, although it should not be taken as the radial distribution itself. The invariability of the shape of the $\Phi(R)$ with increasing Si concentration in the polycrystalline films is evidenced by noting that any spectrum can be transformed to another multiplying it by a constant, as shown in Figs. 12(b) and 13(b). Such a similar loss in amplitude of the XAFS signal has been observed in ball milling pure iron[34] and in amorphous carbon.[35] In the former case, the loss in amplitude was attributed to the increasing density of defects in the crystallites. In the case of amorphous carbon, it was associated to the presence of a very disordered form of carbon whose EXAFS oscillations were strongly dumped. As already commented in the previous section, the spectra of the pure Fe or pure Co thin films had the same shape as the spectra of the films with signifi-

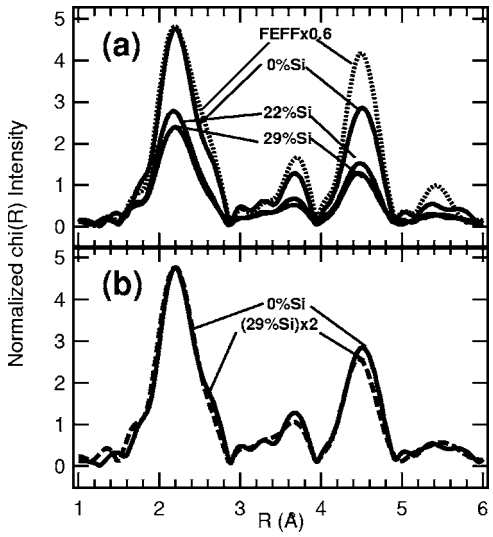

FIG. 12. (a) Comparison of the $\chi(R)=F[k^2\chi(k)]$ spectra of the polycrystalline Fe-Si thin films with different at. Si concentrations, and the theoretical $\chi(R)=F[k^2\chi(k)]$ spectrum of pure bcc-Fe, calculated by FEFF810 (Ref. 39) including the effect of the temperature, muliplied by 0.6. (b) Comparison between the $\chi(R)$ spectrum of the pure Fe film and that of the polycrystalline Fe-Si film with 29% at. Si concentration multiplied by 2.

cant concentrations of Si in them. This already indicates, in a qualitative way, that the TM-Si environment contributed little to the EXAFS spectra. In fact, the TM-Si scattering events were found to have a negligible effect in the fits of the spectra. Table I summarizes the parameters used to fit the spectra of the Fe-Si and Co-Si films, which show more quantitatively all these observations.

Fits of the spectra were done using the IFEFFIT program.[36] The EXAFS oscillations $\chi(k)$ were isolated using the AUTOBK routine,[37] which has been proven to be suitable for this kind of material.[12,38] The fit of the experimental $\chi(k)$ was done from $k_{min}=2$ Å^{-1}, i.e., about 50 eV above the absorption edge. The number of shells used in the fits were four. The parameters obtained for further shells were unreliable because the scattering intensity was too small at those distances, and it was mixed with possible multiscattering events. Actually, multiscattering events between atoms of the first shell were even more intense than the single scattering from the second shell.

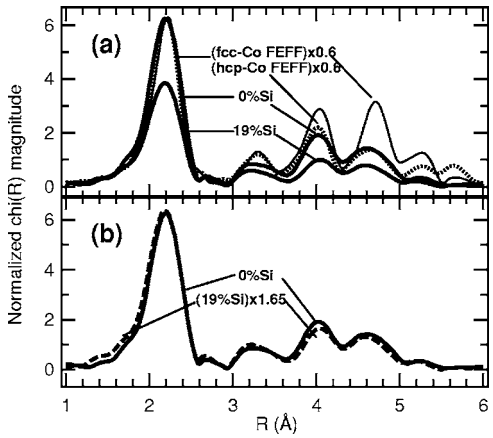

FIG. 13. (a) Comparison of the $\chi(R)=F[k^2\chi(k)]$ spectra of the polycrystalline Co-Si thin films with different at. Si concentrations, and the theoretical $\chi(R)=F[k^2\chi(k)]$ spectra of pure fcc-Co (grey line) and hcp-Co (dashed line), calculated by the FEFF8.10 code (Ref. 39) including the effect of temperature, muliplied by 0.6. (b) Comparison between the $\chi(R)$ spectrum of the pure Co film and that of the polycrystalline Fe-Si film with 19% at. Si concentration multiplied by 1.65.

TABLE I. Parameters used for the fits of the polycrystalline Fe-Si and Co-Si thin films. S_0^2 was obtained considering the actual coordination of the pure bcc-Fe and fcc-Co crystals; R: interatomic distance; σ^2: Width of the Gaussian distribution. k_{min} in the fits was 2 Å^{-1}.

Fe-Si films	Fe-Fe			
Si at. conc.	Shell	S_0^2	R	σ^2
0%	1^{st}	0.60(5)	2.46(2)	0.0028(3)
	2^{nd}	0.60(5)	2.85(2)	0.0028(3)
	3^{rd}	0.60(5)	4.03(3)	0.006(1)
	4^{th}	0.60(5)	4.72(3)	0.006(1)
22%	1^{st}	0.35(5)	2.45(2)	0.0027(5)
	2^{nd}	0.35(5)	2.83(2)	0.0027(5)
	3^{rd}	0.33(5)	4.01(3)	0.006(1)
	4^{th}	0.2(1)	4.7(1)	0.004(2)
29%	1^{st}	0.27(5)	2.45(2)	0.002(1)
	2^{nd}	0.27(5)	2.83(2)	0.002(1)
	3^{rd}	0.24(5)	4.01(3)	0.005(1)
	4^{th}	0.2(1)	4.7(2)	0.003(2)
Co-Si films	Co-Co			
Si at. conc.	Shell	S_0^2	R	σ^2
0%	1^{st}	0.70(5)	2.49(1)	0.0039(3)
	2^{nd}	0.60(5)	3.52(1)	0.006(1)
	3^{rd}	0.35(5)	4.3(1)	0.004(2)
19%	1^{st}	0.46(5)	2.48(1)	0.004(1)
	2^{nd}	0.36(5)	3.5(1)	0.006(1)
	3^{rd}	0.38(5)	4.2(1)	0.008(2)

EXAFS spectra were fitted with the function $\chi(k)$: $\chi(k)=\Sigma_j[N_jS_0^2f_j(k)/kR_j^2]e^{-2\sigma_j^2k^2}e^{-2R_j/\lambda(k)}\sin[2kR_j+\phi_j(k)]$

N_j was the number of atoms of j type around the absorbing atom, S_0^2 was a correction factor to the elastic scattering model, $f_j(k)$ was the backscattering amplitude function of atoms of type j around the absorbing species, R_j was the distance between the absorbing atom and the atom of type j, $e^{-2\sigma_j^2k^2}$ was the Debye-Waller factor, $e^{-2R_j/\lambda(k)}$ was a mean free path term that takes into account the inelastic losses, and $\phi_j(k)$ was the total phase shift in the electron scattering. The functions $f_j(k)$, $e^{-2R_j/\lambda(k)}$ and the total phase shift $\phi_j(k)$ were calculated using the FEFF8.10 code.[39] The parameters to fit for each shell j were the number of atoms N_j, the distance R_j,

and the width of the Gaussian distribution represented in the Debye-Waller factor by σ_j.

As remarked before, the fits showed that TM-Si scatterings were not significant. Spectra fitted properly using TM-TM scattering events only. This agrees with the observed persistence of the shape of the spectra with increasing Si concentration. It is also consistent with XANES qualitative analysis, where the polycrystalline silicide structure seemed to be the sum of the pure TM phase plus a strongly disordered silicide phase. The Fe-Si environment is more visible in the XANES part of the spectra because is for such a range of energies where the electron scattering with Si is stronger than with the Transition Metals. The distribution of atoms around the crystalline sites was assumed to be Gaussian. The coordination numbers and the Debye-Waller factors for each cell were those that fitted $k^n\chi(k)$ of each EAXFS spectra for $n=1$, 2, and 3. This avoided correlation between the coordination number and the Debye-Waller factor since only the coordination number is independent of k.[38].

For the Fe-Si polycrystaline films, given the symmetry of the bcc-Fe structure, only one parameter was varied to adjust the distances of the atoms in the four shells. In the case of the Co-Si films, the two crystalline forms of Co, hcp, and fcc, were modeled. Hcp structure is the most stable phase of Co. But it becomes the more symmetric fcc phase if the stacking of the atomic planes in the hcp c axis is of the type ABCABC instead of ABABAB. This means that their EXAFS spectra are very similar. The single significant difference between both structures is a Co-Co scattering at an interatomic distance of 4.07 Å only present in hcp Co. Such a scattering did not adjust well in the fits. What might probably happen is that disorder, likely due to stacking faults and vacancies, makes the distinction between the two phases difficult for EXAFS, yielding the more symmetric fcc-Co phase. Therefore, only one parameter was varied to adjust the distances of the atoms in the three shells, as it was done in the case of the polycrystalline Fe-Si films.

The empirical parameter S_0^2 showed in Table I is used to correct the losses due to multielectron excitations which are not accounted for in the elastic scattering model used to fit the spectra.[40,41] This parameter was calculated assuming that the coordination was that of bcc-Fe and fcc-Co. The values of this parameter obtained in the fits of the pure metal thin films were a bit lower than reported for these metals, which are found between 0.7[41] and 0.8.[34] S_0^2 for Co was 0.7 and 0.6 for Fe. This could be due to disorder caused by an imperfect crystal growth as evidenced by the increasing width of the Gaussian distribution for the second and third shells. It could be speculated that the lower value of S_0^2 in Fe could be attributed to its higher reactivity with the substrate, that would lead to the formation of an amorphous layer at the interface between the metallic layer and the substrate. The Fe atoms in such an amorphous structure would yield a lower effective coordination in the EXAFS spectra, reducing the total coordination. Since Co reacted less with the substrate, such a virtual reduction of the coordination was lower.

The width of the Gaussian distributions used in the fits did not vary too much with the increasing Si content. But the S_0^2 values decreased significantly when Si concentration increased. This is equivalent to an effective reduction of the coordination of Fe atoms. This effect is very similar to the reported for defective nanocrystalline Fe,[34] implanted Fe in Si crystals,[13] liquid Pb[18] and amorphous carbon.[35] In this case, the loss in coordination can be explained with the model deduced from the analysis of the XANES spectra of the polycrystaline films: The TM atoms were in its pure metal environment and in others disordered Si-rich environments. As Si concentration increased in the film, more TM atoms would form part of the disordered silicide. Since TM-Si scattering events were not detected, Si did not substitute Fe or Co in their corresponding crystalline structures, as it would be the case in a solid solution of Si in these metals,[42] but it occupied very random positions in the material, acting as if it was a vacancy. The number of such "effective" vacancies induced per Si atom, calculated from the decrease in effective coordination number with Si concentration, was estimated in at least two. Coordination numbers decreased to 50% of the expected in bcc-Fe in the most silicided Fe-Si film, taking S_0^2 equal to 0.6, the value obtained in the pure Fe film. This is about what the bcc structure could hold if this decrease in the coordination number was due to an increasing number of vacancies.[34]

EXAFS results were in good agreement with diffraction data. The position of the diffracted peaks in the Fe-Si and Co-Si films agrees with the interatomic distances obtained by EXAFS. Also, the loss in intensity of the $\langle 110 \rangle$ peak in the Fe-Si films with increasing Si concentration, without changes in the texture of the films, can be explained admitting the presence of a very disordered TM-Si phase which coexist with the TM crystalline phase, as deduced from XANES. The loss in diffracted intensity was less important in the Co-Si films because they were less textured. Therefore, the loss of the EXAFS amplitude in the case of the Co-Si polycrystalline films can be interpreted in the same terms than in the case of the Fe silicide polycristalline films. The exact spatial distribution of this amorphous phase cannot be determined from these techniques. Since the width of the diffracted peaks did not change with Si concentration, either the number of crystallites in the film of the size defined by that width decreased, i.e., the disordered phase would segregate from them, or it would be homogeneously distributed in the grains, acting as lattice defects like vacancies in the crystallites.

2. Amorphous Fe-Si *films*

Figure 14 compares $\Phi(R)$ of two films, one amorphous and the other polycrystalline, where the polycrystalline film had about 10% less Si than the amorphous one. The intensity of $\Phi(R)$ of the amorphous film is about four times smaller than that of the polycrystalline silicide film. $\Phi(R)$ has the most intense peak centered about the interatomic distance between first neighbors and intensity from second neighbors is almost negligible. $\Phi(R)$ is shifted to values of R lower than in the polycristalline samples, indicating a shortening of distances between first neighbors. The comparison between the $\Phi(R)$ of all the Fe-Si amorphous films in Fig. 14 shows that the sample with the smallest intensity is the one with the lowest Si concentration (38%), and the intensity of $\Phi(R)$ increases with Si concentration.

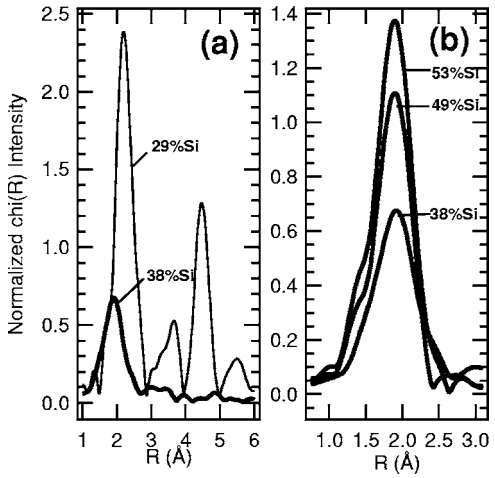

FIG. 14. (a) Comparison of the $\chi(R)=F[k^2\chi(k)]$ spectra of the polycrystalline Fe-Si thin films with 29% at. Si concentration (grey line), and that of the amorphous Fe-Si thin film with 38% at. Si concentration (black line). (b) Comparison between the $\chi(R)$ spectra of the amorphous Fe-Si thin films with different at. Si concentrations.

One of the problems to fit the EXAFS spectra of amorphous substances is that the radial distribution of atoms is not known *a priori*, compared to crystalline structures where Gaussian distributions are proven to be valid. This problem is worsened by the lack of reliable data at low values of the scattering k vector in the EXAFS spectra, hiding information of the points of the atomic distribution function which are at large correlation distances. Asymmetric distribution functions are used in metallic glasses, liquid metals, and binary alloys,[23] where it is assumed that the arrangement of atoms is dominated by excluded volume effects (the DRPHS model). This model might not work properly in amorphous where there are covalent bonds, like those between the TM and Si,[43,44] and local order could be preserved. In the present work, asymmetric distribution functions used to fit other amorphous substances[12,22,23,45] never yielded fits in our spectra better than if Gaussian distributions were utilized. We also found that restricting the fits for k values higher than 4 $Å^{-1}$ produced arbitrary coordination numbers, in the sense that significant changes in the coordination produced fits of similar quality.

Figure 15 shows the EXAFS spectrum of the less silicided amorphous Fe-Si film fitted using three different models. All of them adjusted with equivalent misfits for k higher than 4 $Å^{-1}$. The results of the fits are in Table II. The first model was similar to the one used to fit the EXAFS spectra of amorphous Fe-Co-Si-B ribbons [12]: the Fe atoms were assumed to be asymmetrically distributed, whereas the Si were symmetrically distributed around the Fe atoms. Both the coordination and the width of the distribution for each environment were free parameters. The skew of the distribution, σ_D, was varied until the coordination matched the stoichiometry of the alloy. In the second model, Gaussian distributions were assumed for both kinds of environments. The fit was done for k higher than 4 $Å^{-1}$. The adjustment of this model was slightly better than the previous. However, the coordination was much lower. Note that the EXAFS amplitude of this

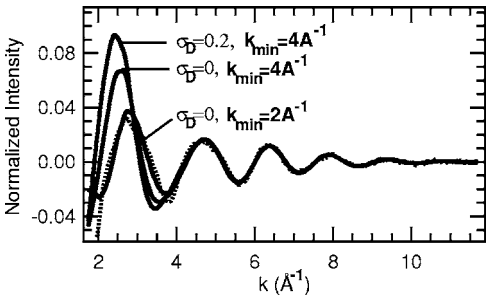

FIG. 15. Fits to the EXAFS oscillations of an amorphous Fe-Si film using three different models. The parameter σ_D is the skew of the atom distribution around the central atom. k_{min} is the lowest k-vector used in the fits. The parameters used in the fits are in Tables II and III. The fitted EXAFS spectrum is that of the amorphous Fe-Si film with 38% Si at. (dashed line).

two resulted fits extrapolated to the region between $k=2$ $Å^{-1}$ and $k=4$ $Å^{-1}$ was significantly higher than the experimental spectrum, as it can be appreciated in Fig. 15. Such a misfit was larger in the model that used an asymetrical distribution for the Fe-Fe environments. The third model was similar to the second, but the k range was expanded up to $k=2$ $Å^{-1}$. The method used to reduce the correlation between the Debye-Waller factor and the coordination number was equivalent to the one utilized for adjusting the spectra of the polycrystalline films. The quality of the fit was the best, although the coordination numbers were even much smaller (see Table III). It should be remarked that, despite such differences in coordination numbers obtained by the three models, all of them yielded qualitatively similar conclusions: Fe atoms distributed at further distances from the central Fe atom than Si atoms did.

The model finally adopted to fit all the spectra of the amorphous films was the third one. The reasons to use a cutoff for k at 4 $Å^{-1}$ are basically the low reliability of the background removal for such low k values and the validity of theoretical approximations in the calculation of the scattering events.[22] However, the spectra of the polycrystalline films were reasonably adjusted for k below 4 $Å^{-1}$ as it has been done in other similar systems[34] and using the same theoretical calculations and background treatments.[38] The fitting of the polycristalline films showed that a significant amount of matter did not contribute with a measurable amplitude to the EXAFS oscillations, i.e., its signal was effectively dumped

TABLE II. Parameters used for the fits of the amorphous Fe -Si thin film with 38% at. Si concentration, for $k_{min}=4$ $Å^{-1}$ using two different values for σ_D (see text and Fig. 15). S: Standard deviation of the fit; N: Coordination number (using $S_0^2=1$); R: Interatomic distance; σ^2: Width of the Gaussian distribution; σ_D: Skew of the distribution (mean deviation of interatomic distance).

	Fe-Fe				Fe-Si		
S	N	R	σ^2	σ_D	N	R	σ^2
1.5×10^{-3}	6(1)	2.46(1)	0.013(7)	0.2	3.5(6)	2.40(1)	0.01(1)
0.9×10^{-3}	2.8(5)	2.54(1)	0.013(5)	0	2.8(6)	2.38(1)	0.015(7)

TABLE III. Parameters used for the fits of the amorphous Fe-Si thin films. S: Standard deviation of the fit; N: Coordination number (using $S_0^2=1$); R: Interatomic distance; σ^2: Width of the Gaussian distribution. PEP: Magnetic anisotropy parallel to the evaporation plane. AEP: Magnetic anisotropy antiparallel to the evaporation plane. k_{min} in the fits was 2 Å^{-1}.

Fe-Si *films* Si at. conc.	S	Fe-Fe			Fe-Si		
		N	R	σ^2	N	R	σ^2
38% PEP	3.4×10^{-3}	0.4(2)	2.54(1)	0.003(3)	1.2(2)	2.30(1)	0.006(3)
49% AEP	2.6×10^{-3}	0.0(2)	—	—	2.32(1)	2.35(1)	0.006(2)
53% AEP	3.1×10^{-3}	0.7(9)	2.74(3)	0.01(1)	3.3(2)	2.36(1)	0.008(1)

for all the spectral k range attained by EXAFS, demonstrating that this spectroscopy is only sensitive to very short range distances and local order.[22] Another reason to adopt that same model than the used for the polycrystalline films was to keep coherence in the analysis. This model assumed that the coordination obtained from the fits was not real but a measure of the effective disorder of the analyzed matter.

The parameters used in the fits are shown in Table III. The most remarkable results are:

(a) The extraordinary small coordination numbers, only a bit higher than 3 for the Fe-Si environment in the most silicide sample, and less than 1 for the Fe-Fe environment in the least silicide sample. This can be followed from the strong damping of the EXAFS signal from the polycristalline silicide to the amorphous state showed in Fig. 14. The reduced coordination in all the films cannot be due to the presence of voids or similar kind of defects because their density measured as a function of their thickness deduced from x-ray reflectometry was not significantly reduced.

(b) The need of Fe-Si environments in the fits, undetectable in the poly-crystalline films. Actually, this environment had the highest contribution to the spectra, i.e., it had the highest coordination numbers in all the samples.

It is recalled that the coordination number obtained from this analysis depends on the disorder degree of the corresponding environment: The higher the disorder the smaller its contribution to the EXAFS amplitud and, therefore, its coordination number. If the studied alloys were not homogeneous but they consisted on a mixture of phases with different atomic environments, only those with the lowest disorder would have a higher coordination, i.e., they will be more visible by EXAFS. The fact that only the pure TM-TM environments fitted the polycrystalline films, and that Gaussian functions fitted better with the spectra of the amorphous samples, should be an indication that the observed EXAFS amplitude in the amorphous samples comes from certain Fe environments with a higher order than others that would have a poor contribution to the EXAFS spectra.

The increase in the contribution of the Fe-Si environment was not linear with the increase in Si concentration, what it would mean that Fe-Si environments precipitate or segregate in these alloys. When Si concentration increased in less than 10%, the increase in coordination number of the Fe-Si environment was of about 100% whereas the Fe-Fe environment practically vanished. It is remarkable that the width of the Gaussian distribution did not changed from one sample to another. This would be consistent with a precipitation of Fe-Si environments. Also, the Fe-Si interatomic distance changed from 2.30 to 2.35 Å. This last interatomic distance is similar than the found in crystalline $FeSi_2$ (see Table V). Another equivalent increment of Si concentration in the composition of the amorphous alloy rended it almost nonferromagnetic. The Fe-Si environment incremented notably in coordination, without a significant change in its interatomic distance. The Fe-Fe environment contribution was weak. It increased its coordination but accompanied by a rather high Debye-Waller factor. In this case, its interatomic distance was increased substantially to values closer to that of Fe in $FeSi_2$. Figure 16 shows graphically the contributions of each

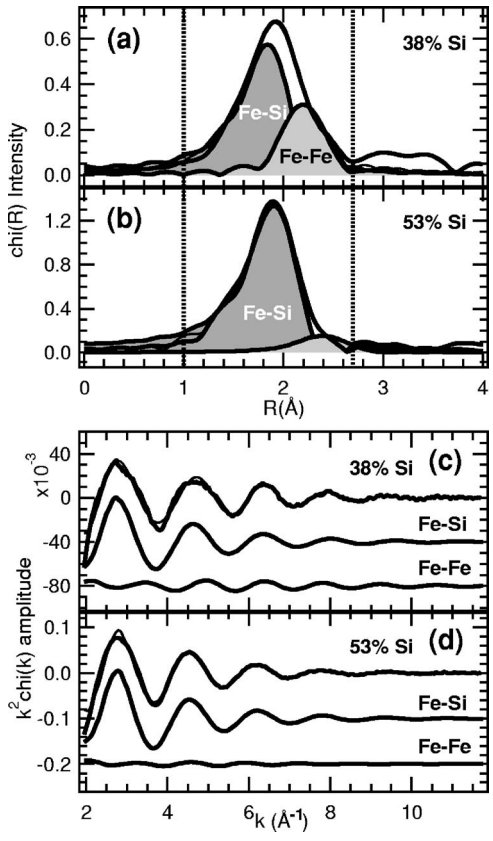

FIG. 16. Contributions of the Fe-Fe and Fe-Si environments to the EXAFS spectra of two different amorphous Fe-Si thin films: (a) and (c) 38% at. Si concentration and (b) and (d) 53% at. Si concentration. The thin line is the fitting function.

of the environments to the spectra. This Fe-Si environment was not magnetic since it was most intense in the least ferromagnetic film. Therefore, it should be differentiated from other necessarily magnetic Fe-Si and Fe-Fe environments, whose contribution to the EXAFS signal was too small to be detected likely because they were highly disordered. It is remarkable that no Fe-Fe environments were detected at distances below 2.5 *Å* despite that all the crystalline phases of Fe silicide that are magnetic have Fe-Fe environments at such distances.

Fe-Si environment segregation in these alloys is expected from their phase diagram. Outside the concentration at the eutectic point, the tendency is to segregate the phases with the most simple structure.[5,13] The most relevant case, connected with the case presented here, is that of Fe-Ge whose homogeneity was studied by XANES and Small Angle X-ray Scattering (SAXS).[7] The study found that the alloys contained inhomogeneities at concentrations between 33% at. Fe, i.e., the concentration of $FeGe_2$, and 72% at. Fe, near the concentration of Fe_5Ge_3 and Fe_3Ge. For such concentrations, phase separation of $FeGe_2$ and Fe_3Ge occurred. A similar behavior might happen in the films studied in our work. The crystalline phases for Fe-Ge are equivalent to those of Fe-Si.

The magnetic properties of coercivity and anisotropy could be understood taking into account such a segregation of Fe-Si environments with increasing Si concentration. The sample with the lowest effective coordination, i.e., the most atomically disordered, was the one with the concentration of the eutectic point, as expected. It was also the sample with the lowest coercivity and anisotropy energy. This suggest that the density of defects that would difficult domain wall displacement was low, as it was also deduced from its hysteresis loops of Fig. 3. This sample would be the most homogeneous. It was the only one that had the highest contribution from Fe-Fe environments at short distances, of the order of 2.54 Å. The control of the orientation of the magnetic anisotropy easy axis of these kind of samples with relatively weak magnetic fields externally applied during the growth could be explained in base of these Fe-Fe environments. Their magnetic anisotropy would arise by either the orientation of pairs of Fe moments along the direction of the applied magnetic field. It might be also due to the orientation of small bcc-Fe clusters scarcely present in the film.[3] The diffraction characterization previously presented showed that the amorphous film with the highest PEP anisotropy had a non-negligible intensity at the bcc-Fe reflection at about 44° [see Fig. 5(b), the diffraction pattern of the sample with 38% at. Si].

For higher Si concentrations the anisotropy direction changed to be perpendicular to the evaporation plane, suggesting that structural changes occurred in the film due to atom diffusion and segregation process induced by the oblique angle of incidence of the evaporated Si atoms.[4] The segregation of nonmagnetic Fe-Si environments evidenced by EXAFS might indicate that these Fe-Si environments would be large enough to cluster in larger areas delimiting other regions rich in Fe and, therefore, magnetic. This would produce a modulation in the concentration of Si, and therefore, in the distribution of the magnetic regions, that would have a shorter period in the direction parallel to the evaporation plane. Then the observed anisotropy in this range of concentrations would be explained by the resulting anisotropic magnetic interaction between the magnetic regions of the film. The sizes of the phase separated regions are unknown from the present experiments. Such a kind of phase separation has been observed in Fe-Si and Fe-Ge alloys,[16] although in the range of atomic concentrations were Si was majority. In that case, the phase separated regions were in the nanometer scale.

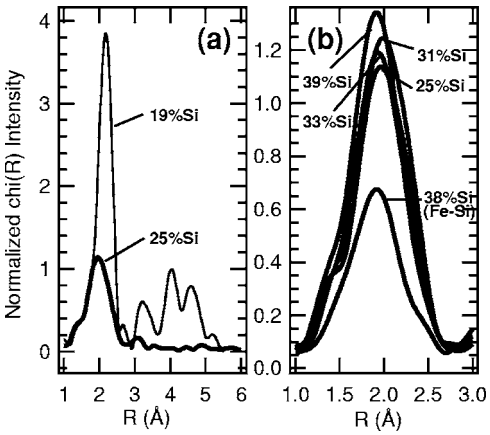

FIG. 17. (a) Comparison of the $\chi(R)=F[k^2\chi(k)]$ spectra of the polycrystalline Co-Si thin films with 22% at. Si concentration (grey line), and that of the amorphous Co-Si thin film with 25% at. Si concentration (black line). (b) Comparison between the $\chi(R)$ spectra of the amorphous Co-Si thin films with different at. Si concentrations and that of the amorphous Fe-Si thin film with 38% at. Si concentration.

3. Amorphous Co-Si

Figure 17 compares the $\Phi(R)$ obtained from the EXAFS spectra of the amorphous Co-Si films with the $\Phi(R)$ of the amorphous Fe-Si film with the lowest Si concentration. Clearly, the amplitude of EXAFS oscillations was higher in the amorphous Co-Si films than in the Fe-Si films. The spectra of the Co-Si films showed little variations in amplitude with increasing Si. This was reflected in the parameters obtained from the fits, resumed in Table IV. The corresponding contributions of the Co-Co and Co-Si environments to the spectra, as resulted from the fits are displayed in Fig. 18. The fits were done in a similar way than those of Fe-Si. Two different environments, Co-Co and Co-Si, were used for the fits. Atoms were considered to be distributed following a Gaussian function which, again, yielded better fits than asymmetric atomic distributions.

The mean interatomic distance between first neighbors was almost constant for the Co-Si environments, of about 2.29 Å. The only crystalline phase of Co-Si that has Si atoms distributed at so close distances around Co atoms is $CoSi_2$, where the interatomic Co-Si distance is 2.32 Å (see Table VI). On the other hand, the interatomic distance of the Co-Co environment increased its value progressively, from 2.52 to 2.57 Å in the nonferromagnetic film. There is not a single crystalline phase of Co-Si with the first neighbors at such distances. This suggest that the Co-Co and Co-Si envi-

TABLE IV. Parameters used for the fits of the amorphous Co-Si thin films. S: Standard deviation of the fit; N: Coordination number (using $S_0^2=1$); R: Interatomic distance; σ^2: Width of the Gaussian distribution. AEP: Magnetic anisotropy antiparallel to the evaporation plane. N-M: No magnetic. k_{min} in the fits was 2 $Å^{-1}$.

Co-Si *films* Si at. conc.	S	Co-Co			Co-Si		
		N	R	σ^2	N	R	σ^2
25% AEP	3.0×10^{-3}	2.8(9)	2.52(1)	0.012(3)	1.2(2)	2.28(2)	0.004(2)
31% AEP	1.7×10^{-3}	2.5(5)	2.50(1)	0.009(2)	1.3(2)	2.29(1)	0.004(2)
33% AEP	1.6×10^{-3}	1.7(5)	2.54(1)	0.008(3)	1.5(2)	2.28(1)	0.004(2)
39% N-M	2.8×10^{-3}	1.5(7)	2.57(1)	0.007(5)	2.1(3)	2.29(1)	0.005(2)

ronments might not be found with the same central Co atom, but it might correspond to two possible environments where it is possible to find the Co atom.

The crystalline phases of Co-Si with Co-Co bond distances closer to the one obtained from the fits were hcp-Co and Co_2Si which is not ferromagnetic (see Table VI). Its crystalline structure is a bit complex and each Co has its first Co neighbors almost uniformly distributed between 2.50 and 2.68 Å. So if Co-Co corresponded to such a kind of environment, its interatomic distance would be displaced to higher values. Actually, such displacement, from 2.50 to 2.57 Å, happened with the increasing Si concentration. Other crystalline forms of cobalt silicides, like CoSi and $CoSi_2$, have too large distances between first Co neighbors, of 2.74 and 3.8 Å respectively. Therefore, the Co-Co environments might correspond to environments of the type found in hcp-Co, with increasing contribution from Co-Co environments similar to those of the crystalline phase of Co_2Si with increasing Si content.

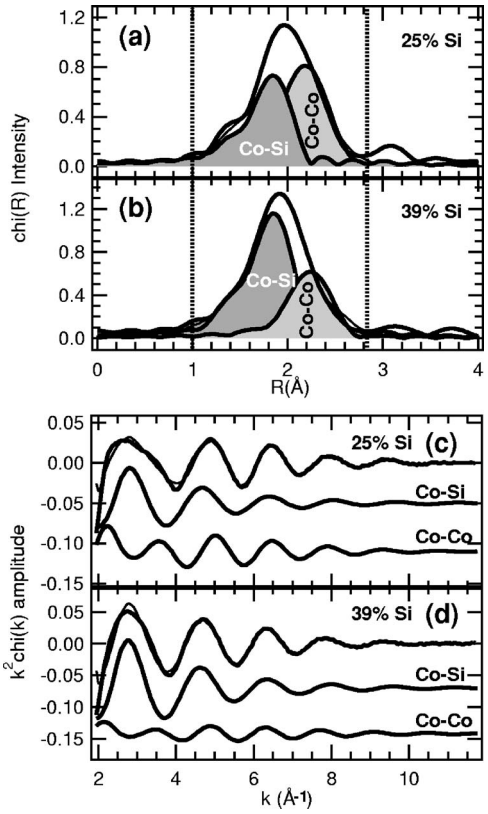

FIG. 18. Contributions of the Co-Co and Co-Si environments to the EXAFS spectra of two different amorphous Co-Si thin films: (a) and (c) 25% at. Si concentration and (b) and (d) 39% at. Si concentration. The thin line is the fitting function.

The bar diagrams in Fig. 19 compare the coordination deduced from the EXAFS fits ("EXAFS coordination") and the "effective contribution" of TM-TM and TM-Si environments to the EXAFS spectra of the Co and Fe amorphous silicides. The "effective contribution" was defined as the ratio between the coordination and the width of the Gaussian distribution. The most important difference between the two alloys is the much higher coordination and contribution of the Co-Co environment in the Co-Si films compared to the Fe-Fe environment in the Fe-Si films. Also, for similar Si concentrations, the Co-Si environment is more intense than the Fe-Si environment suggesting a higher precipitation of $TMSi_2$ in the Cobalt silicide than in the Iron silicide alloys. Note that the sample with the lowest Fe-Si coordination and "efective contribution" to EXAFS is the Iron silicide sample whose magnetic anisotropy is PEP.

A higher Co-Co segregation should be found in the amorphous Co-Si films than in the Fe-Si films because their different heat of mixing,[8,11] and this is reflected in the higher effective coordination of the Co-Co environments. The assignation of the Co-Co magnetic environments in the amorphous magnetic films to one similar than in hcp-Co agrees with the conclusions obtained from the analysis of their corresponding XANES spectra, which fitted to the sum of the spectrum of pure Co (hcp-Co) and that of the most silicide film (see Fig. 11). It is recalled that such a kind of fit was worse in the case of the Fe-Si films, evidencing a better mixing of Fe with Si than in the case of the Co-Si amorphous films.

The magnetic anisotropy axis of the amorphous Co-Si films resulted to be always in the plane of the sample and perpendicular to the plane of incidence of evaporated species, i.e., in the same direction than the Si rich amorphous Fe-Si films (AEP samples). Therefore, the origin of the anisotropy in these films should be similar than in the AEP Iron silicide films, i.e., there should be an anisotropic interaction between the different magnetic regions of the film due to a spatial modulation in the concentration of Si induced by the

TABLE V. First neighbors radial distribution around the Fe atom in the most common Iron and silicide forms. FM: Ferromagnetic; NM: No ferromagnetic.

Phase	Fe-Fe	N_{Fe}	Fe-Si	N_{Si}
fcc Fe FM	2.58 Å	12	—	—
bcc Fe FM	2.48 Å	8	—	—
	2.87 Å	6	—	—
Fe_3Si FM	2.45 Å	8	2.82 Å	6
Fe_5Si_3 FM	2.35 Å	2	2.37 Å	6
FeSi NM	2.76 Å	6	2.27 Å	1
	—	—	2.35 Å	3
	—	—	2.50 Å	3
$FeSi_2$ NM	2.68 Å	4	2.35 Å	8

oblique angle of evaporation. It was argued in the previous section that the presence of Fe-Fe environments found only in the PEP Fe-Si sample indicated that these environments were directly involved in the orientation of the easy axis of this sample. As pointed out before, the Co-Co environment is more intense in the amorphous Co silicide films than in the amorphous PEP Fe-Si film. Therefore, another possibility is that the *c-axis* of the possible small hcp-Co clusters or Co -Co atom pairs were oriented along the direction perpendicular to the evaporation plane. If that was the case, the easy axis direction should be reoriented with externally applied magnetic fields during film growth, as it was done with the PEP Iron silicide films. In that case, less than 30 Oe of applied magnetic field were enough to reorientate the easy axes. Such a field did not induce an easy axis reorientation in any amorphous Cobalt silicide sample. What it could explain the absence of amorphous Co-Si films with PEP anisotropy, like in the lowest silicide amorphous Fe-Si films, is that the amorphous Co-Si films are less homogeneous than the amorphous PEP Fe-Si films. This could be the case because the larger contribution of the Co-Si environment to the EXAFS spectra for Si concentrations much lower than in the most disordered Fe-Si sample (see Fig. 19).

TABLE VI. First neighbors radial distribution around the Co atom in the most common Iron and silicide forms. FM: Ferromagnetic; NM: No ferromagnetic.

Phase	Co-Co	N_{Co}	Co-Si	N_{Si}
fcc Co FM	2.51 Å	12	—	—
hcp Co FM	2.50 Å	6	—	—
	2.51 Å	6	—	—
Co_2Si NM	2.50 Å	2	2.34 Å	2
	2.53 Å	1	2.47 Å	1
	2.59 Å	2	2.57 Å	2
	2.66 Å	3	—	—
CoSi NM	2.74 Å	6	2.29 Å	1
	—	—	2.34 Å	3
	—	—	2.49 Å	3
$CoSi_2$ NM	3.79 Å	12	2.32 Å	8

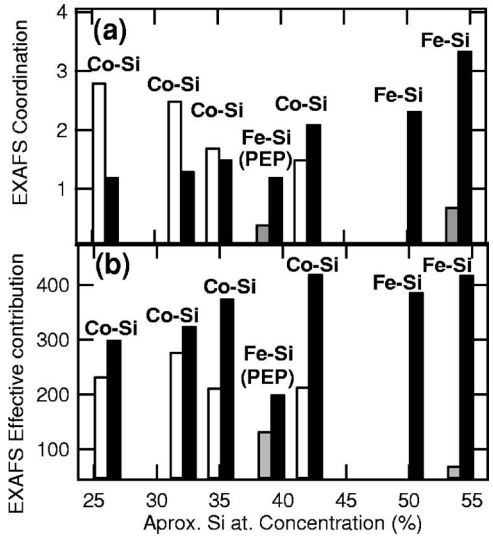

FIG. 19. (a) Comparison of the coordination numbers obtained from the fits of the EXAFS spectra of the analyzed amorphous films and (b) the "effective contribution" to the EXAFS spectra of Co -Co (white), Fe-Fe (grey), and TM-Si (black) environments.

IV. CONCLUSIONS

Fe-Si and Co-Si magnetic films deposited by magnetron sputtering with different Si concentrations were studied by x-ray diffraction and x-ray absorption spectroscopy to understand its structure and correlate it with their magnetic properties, especially their magnetic anisotropy.

The polycrystalline silicide films resulted to be the combination of the pure transition metal and a second phase consisted in a highly disordered form of silicide that gave a practically negligible EXAFS signal.

The complete reduction of the pure transition metal polycrystal occurred at the eutectic point, where the amplitude of the EXAFS signal was the lowest. Such a TM reduction was stronger in the case of the Fe-Si films, where it was almost complete, than in the Co-Si films. This indicated that the mixing of the TM with Si in the amorphous films was higher in Fe-Si than in Co-Si as it would be expected from the higher heat of mixing of Fe with Si.

The amorphous Fe-Si films was the combination of two phases: one detected by EXAFS that consisted in Fe-Si environments similar to the found in $FeSi_2$, which highly increased its intensity when Si concentration was increased. The second phase was hardly detected by EXAFS and it should consist in a strongly disorder silicide form, which should be forcedly magnetic since $FeSi_2$ is not magnetic.

Such a $TMSi_2$ segregation occurred as well in the Co-Si amorphous films, where the Co-Si environments related to $CoSi_2$ dominated their EXAFS spectra. The main difference with respect to the amorphous Fe-Si films was the higher presence of Co-Co environments. Such environments were associated to pure Co that kept unmixed with Si for low concentrations of Si. For higher Si concentrations, the Co -Co environments increased their interatomic distances, approaching those of Co_2Si. Therefore, the most amorphous Co-Si films should be the combination of segregated $CoSi_2$

and pure Co environments plus a highly disordered silicide form that contributed very little to the EXAFS spectra.

These results confronted to the magnetic anisotropy of the films suggest that this was originated by the anisotropic distribution of Si in them. This model could not be applied to the Fe-Si amorphous film with the lowest Si concentration, which had the anisotropy parallel to the evaporation plane instead of perpendicular like in the rest of the films. This was the most disordered film as deduced from the amplitude of their EXAFS oscillations, so it was supposed that the spatial distribution of environments was the most homogeneous of all the analyzed films, and its anisotropy was probably induced by atom pair correlations or, perhaps, because of the alignment of a very low concentration of pure Fe crystallites of very small size with magnetic fields externally applied. The absence of such amorphous films with that kind of anisotropy in Co-Si indicates that they should be less homogeneous than the Fe-Si films, what it could be conveyed from the larger contribution of the nonmagnetic Co-Si environments in their EXAFS spectra. XANES and EXAFS spectroscopies are obviously insensitive to the spatial distribution of the different environment contributing to the oscillations, so further experiments based on high resolution microscopy and x-ray scattering should proceed to check such a model.

ACKNOWLEDGMENTS

We acknowledge financial support by the Spanish CICYT with Grants Nos. MAT99-0724 and HF/1999-0041. We acknowledge the European Synchrotron Radiation Facility for provision of the synchrotron radiation facilities and we would like to thank Dr. Stefano Colonna for assistance in using beamline BM8 (Gilda).

*Electronic address: javidiaz@condmat.uniovi.es

[1] T. Kaneyoshi, *Introduction to Amorphous Magnets* (Published by World Scientific Publishing Co. Pte. Ltd., 1992).
[2] R. Alben and J. Becker, J. Appl. Phys. **49**, 1653 (1978).
[3] G. Suran, K. Ounadjela, and F. Machizaud, Phys. Rev. Lett. **57**, 3109 (1988).
[4] O. P. Karpenko, J. C. Bilello, and S. M. Yalisove, J. Appl. Phys. **82**, 1397 (1997).
[5] R. B. Schwarz and W. L. Johnson, Phys. Rev. Lett. **51**, 415 (1983).
[6] C. Lin, G. W. Yang, and B. X. Liu, J. Phys. D **32**, 953 (1999).
[7] R. D. Lorentz, A. Bienenstock, and T. I. Morrison, Phys. Rev. B **49**, 3172 (1994).
[8] K. H. J. Buschow and A. M. van der Kraan, J. Magn. Magn. Mater. **22**, 220 (1981).
[9] K. H. J. Buschow and P. G. van Engen, J. Appl. Phys. **52**, 3557 (1981).
[10] A. M. van der Kraan and K. H. J. Buschow, Phys. Rev. B **25**, 3311 (1982).
[11] A. R. Miedema, P. F. D. Châtel, and F. R. de Boer, Physica B & C **100**, 1 (1980).
[12] M. L. Fdez-Gubieda, I. Orúe, F. Plazaola, and J. M. Barandiarán, Phys. Rev. B **53**, 620 (1996).
[13] Z. Tan, F. Namavar, J. I. Budnick, F. H. Sanchez, A. Fasihuddin, S. M. Heald, C. E. Bouldin, and J. C. Woicik, Phys. Rev. B **46**, 4077 (1992).
[14] M. Vélez *et al.*, IEEE Trans. Magn. **41**, 517–524 (2004).
[15] J. Díaz, N. Hamdan, P. Jalil, Z. Hussain, S. M. Valvidares, and J. M. Alameda, IEEE Trans. Magn. **38**, 2811 (2002).
[16] M. J. Regan, M. Rice, M. B. Fernandez vanRaap, and A. Bienenstock, Phys. Rev. Lett. **73**, 1118 (1994).
[17] J. Díaz, S. M. Valvidares, R. Morales, and J. M. Alameda, J. Magn. Magn. Mater. **242–245**, 166 (2002).
[18] E. A. Stern, P. Livins, and Z. Zhang, Phys. Rev. B **43**, 8850 (1991).
[19] P. Eisemberger and G. S. Brown, Solid State Commun. **29**, 481 (1979).
[20] P. Eisenberger and B. Lengeler, Phys. Rev. B **22**, 3551 (1980).
[21] E. A. Stern, Y. Ma, and O. Hanske-Petitpierre, Phys. Rev. B **46**, 687 (1992).
[22] A. Filipponi, J. Phys.: Condens. Matter **13**, R23 (2001).
[23] A. Trapananti and A. DiCicco, Phys. Rev. B **70**, 014101 (2004).
[24] C. Dehesa-Martínez, L. Blanco-Gutierrez, M. Vélez, J. Díaz, L. M. Alvarez-Prado, and J. M. Alameda, Phys. Rev. B **64**, 024417 (2001).
[25] T. Ishiguro, H. Fujii, Y. Ichinose, J. Endo, and H. Harada, J. Appl. Phys. **61**, 4284 (1987).
[26] J. M. Alameda, M. C. Contreras, and H. Rubio, Phys. Status Solidi A **85**, 511 (1984).
[27] K. J. Harte, J. Appl. Phys. **39**, 1503 (1968).
[28] H. Hoffmann, IEEE Trans. Magn. **4**, 32 (1968).
[29] P. Bruno, Phys. Rev. B **39**, R865 (1989).
[30] C. Mény, E. Jędrica, and P. Panissod, J. Phys.: Condens. Matter **5**, 1547 (1993).
[31] J. M. Fallon, C. A. Faunce, and P. J. Grundy, J. Phys.: Condens. Matter **12**, 4075 (2000).
[32] O. Kitakami, S. Okamoto, and Y. Shimada, J. Appl. Phys. **79**, 6880 (1996).
[33] D. K. Sarkar, M. Falke, H. Giesler, S. Teichert, G. Beddies, and H.-J. Hinneberg, J. Appl. Phys. **89**, 6506 (2001).
[34] A. DiCicco, M. Berrettoni, S. Stizza, E. Bonetti, and G. Cocco, Phys. Rev. B **50**, 12386 (1994).
[35] G. Comelli, J. Stöhr, W. Jark, and B. B. Pate, Phys. Rev. B **37**, 4383 (1988).
[36] M. Neville, B. Ravel, D. Haskel, J. J. Rehr, and Y. Yacoby, Physica B **208–209**, 117 (1995).
[37] M. Newville, P. Livins, Y. Yacoby, J. J. Rehr, and E. A. Stern, Phys. Rev. B **47**, 14126 (1993).
[38] E. A. Stern, R. W. Siegel, M. Newville, P. G. Sanders, and D. Haskel, Phys. Rev. Lett. **75**, 3874 (1995).
[39] A. L. Ankudinov, B. Ravel, J. J. Rehr, and S. D. Conradson, Phys. Rev. B **58**, 7565 (1998).
[40] G. Bunker and E. A. Stern, Phys. Rev. Lett. **52**, 1990 (1984).
[41] A. Bianconi, *X-Ray Absorption: Principles, Applications, Techniques of EXAFS, SEXAFS and XANES*, edited by D. C. Koningsberger and R. Prins (Wiley, New York, 1988) pp. 573–662.

[42] W. A. Hines, A. H. Menotti, J. I. Budnick, T. J. Burch, T. Litrenta, V. Niculescu, and K. Raj, Phys. Rev. B **13**, 4060 (1976).
[43] B. W. Corb, R. C. O'Handley, and N. J. Grant, Phys. Rev. B **27**, 636 (1983).
[44] A. Collins, R. C. O'Handley, and K. H. Johnson, Phys. Rev. B **38**, 3665 (1988).
[45] Y. Takahara and N. Narita, Mater. Sci. Eng., A **315**, 153 (2001).